Construction and Building Materials 409 (2023) 134116

Contents lists available at ScienceDirect

Construction and Building Materials

journal homepage: www.elsevier.com/locate/conbuildmat

# Directionally sensitive cement-based sensor using carbon nanotube and carbonyl iron powder (CNT@CIP)-based nanohybrid clusters

Daeik Jang [a,b], Jinho Bang [c], H.N. Yoon [a], Young-Kwan Kim [d], Jae Hyuk Lee [c], Hyungchul Yoon [c,*], Se-Hyeon Cheon [e,*], Beomjoo Yang [c,*]

[a] Department of Civil and Environmental Engineering, Korea Advanced Institute of Science and Technology (KAIST), 291 Daehak-ro, Yuseong-gu, Daejeon 34141, South Korea
[b] Department of Civil and Environmental Engineering, University of Pittsburgh, Pittsburgh, PA 15261, USA
[c] School of Civil Engineering, Chungbuk National University, 1 Chungdae-ro, Seowon-gu, Cheongju, Chungbuk 28644, South Korea
[d] Department of Chemistry, Dongguk University-Seoul Campus, 30 Pildong-ro, Jung-gu, Seoul 04620, South Korea
[e] School of Spatial Environment System Engineering, Hangdong Global University, 558 Handong-ro, Buk-gu, Pohang, Gyeongbuk 37554, South Korea

ARTICLE INFO

*Keywords:*
Carbon nanotubes (CNTs)
Carbonyl iron powder (CIP)
Nanohybrid clusters
Multi-directional sensors
Long short-term memory (LSTM) model

ABSTRACT

Cement-based sensors have been highlighted for using as structural health monitoring sensors; however, the conventional cement-based sensors can only detect the levels of applied loading not the direction of the loading. Therefore, this study proposes a new method for developing cement-based sensors which can detect the levels of applied loadings with their direction. The proposed method involves using carbon nanotube and carbonyl iron powder (CNT@CIP)-based nanohybrid clusters, which are added to the cement-based sensors during fabrication, and controlling their conductive networks through magnetization curing. The fabricated cement-based sensors are then tested for piezoresistive sensing. The experimental outcomes indicated directional sensitivity values of 3.12%, 2.47%, and 0.98%/MPa stress sensitivity in horizontal, random, and vertical sensors. In addition, their long-term sensing capabilities are predicted using a long short-term memory (LSTM) model. The findings of this study could be useful in developing multi-directional cement-basd sensors and predicting their long-term sensing capabilities.

## 1. Introduction

The development of cement-based sensors have attracted increasing attention which can meet the requirements for structural health monitoring systems due to their various advantages such as simple manufacturing, easy installment, low cost, and high mechanical durability [1–4]. In addition, the cement-based sensors showed the possibility of using as crack monitoring sensors and smart infrastructures [5–7]. To fabricate the cement-based sensors, the conductive fillers have been added to the cementitious composites including metallic materials and carbon-based materials [8–11]. Among the various types of conductive fillers, carbon nanotubes (CNT) have been regarded as the favorable candidate owing to their high electrical conductivity with low amount [12–16]. Mardani et al. added 0.45% of CNT to the cementitious composites, and it showed 43.66 of gauge factor and 0.13 of stress sensitivity [13]. Dong et al. fabricated 0.5% of multi-walled CNT (MWCNT)-embedded cement composites, and it showed 12.5% of fractional change of resistivity as 10 MPa of compressive loading was applied [14].

Based on the previous studies, it can be said that many researchers have attempted to [8–11]improve the dispersion of conductive fillers in the cement matrix [17–22], and many efforts were also given to enhance the sensitivity and durability of the cement-based sensors [23–26]. However, the conventional cement-based sensors are not able to monitoring the direction of applied forces. As the conductive fillers are inherently distributed randomly within the composites, their mobility is solely contingent upon the magnitude of the applied loads [27]. For these reasons, the cement-based sensors with anisotropic conductive fillers-based networks have been proposed by some researchers [28–30]. For example, Tian et al. added nickel powders to the cement and cured under the magnetization, proposing the novel cement-based sensors with magneto-aligned nickel powder [30]. These proposed sensors with differently aligned direction exhibited the different sensitivity even the same applied loading is applied, showing the potential of monitoring the

* Corresponding authors.
*E-mail addresses:* hyoon@chungbuk.ac.kr (H. Yoon), shcheon@handong.edu (S.-H. Cheon), byang@cbnu.ac.kr (B. Yang).

https://doi.org/10.1016/j.conbuildmat.2023.134116
Received 19 April 2023; Received in revised form 21 September 2023; Accepted 6 November 2023

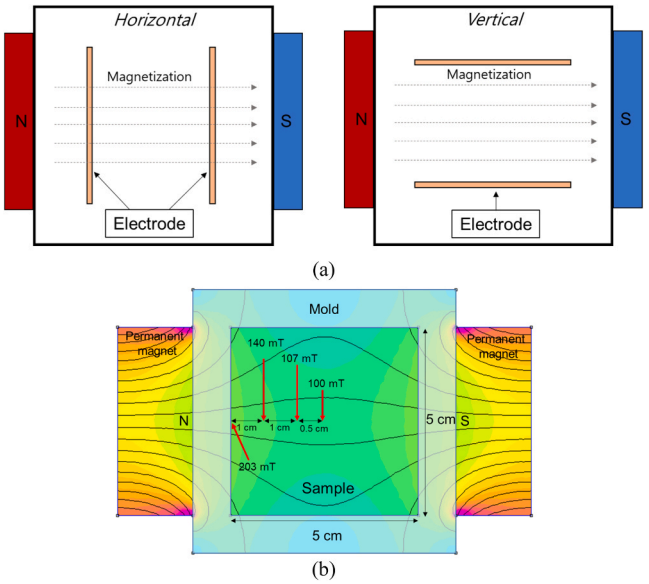


**Fig. 1.** (a) Schematic of the formed CNT@CIP-based conductive networks and (b) simulation of the magnetization method using FEMM software.

direction of applied forces [30]. Meanwhile, a large amount of magnetic and/or nickel powder is required to fabricate the cement-based sensors compared to that fabricated with CNT due to the low electrical conductivity of the magnetic and/or nickel powder. However, in case of CNT-embedded cement-based sensors, it is impossible to align the CNT particles in the sensor to form the anisotropic conductive networks. To solve these limitations, carbonyl iron powder (CIP) was newly used in the present study to form the CNT and CIP (CNT@CIP) nanohybrid clusters. As they were added together, they can form CNT@CIP nanohybrid clusters, which can respond to the external magnetic field, allowing the fabrication of cement-based sensors with aligned conductive fillers [31].

The present study aims to fabricate the cement-based sensors with different directionally aligned CNT@CIP nanohybrid clusters and utilizes the developed sensors for monitoring the both levels and direction of the applied loadings. First, various characterization methods including zeta potential measurement, Fourier-transform infrared (FT-IR) and Raman spectroscopy were conducted to investigate the formation of CNT@CIP nanohybrid clusters. Second, the DC and AC electrical conductivity of the sensors with different aligned direction was examined. Third, their piezoresistive sensing capabilities of the sensors were examined under various loading conditions including monotonic, short-term, and long-term cyclic loading to evaluate the possibility to be utilized as multi-directional sensors in structural health monitoring systems. Lastly, a deep learning model based on long short term memory (LSTM) which shows a superior capability for accurately prediction was utilized to predict the long-term piezoresistive sensing capabilities of the sensors, using the experimental data obtained [32,33].

## 2. Experimental program

### 2.1. Fabrication of samples

To fabricate the CNT@CIP-based nanohybrid clusters-embedded cement-based sensors, 10% of silica fume (Elkem Inc., EMS-970), 0.35% of multi-walled CNT (KUMHO Petrochemical Co., Ltd), 16% of CIP (BASF), 0.5% of polycarboxylate acid-typed superplasticizer (SP) (Dongnam Co., Ltd., FLOWMIX 3000 U), and 40% of water by cement mass were prepared. The sensors was fabricated as follows; first, the solution including water and SP was prepared, and conductive fillers (i.e., CNT and CIP) were added to the prepared solutions. The specification

**Table 1**
Zeta potential values of the CNTs and CIP in water.

| Zeta potential value (mV) | Water | CNT in water | CIP in water | CNTs and CIP in water |
|---|---|---|---|---|
| Absolute values | -34.0 | -17.3 | -47.0 | -27.3 |
| Relative values | 0 | 16.7 | -13.0 | 6.7 |

of the used fillers can be found in the previous study by the authors [31,34]. The prepared mixtures were hand-mixed for 1 min, and sonicated for 1 h using a tip-typed ulatrsonicator (Sonic & Materials, USA) with 50% of maximum amplitude and 10 s of on/off pulse interval. At the same time, the dry mixtures including cement and silica fume were dry mixed for 5 min using a Hobart-mixer. Then, the sonicated mixtures were poured into the dry-mixtures, and they were additionally mixed for 5 min. The total mixtures were poured into cubical molds with 50 mm size. The copper electrodes with 70 mm length and 20 mm width coated with silver paste were embedded into the composites. Then, the permanent magnets were attached to both side of the molds, to form the CNT@CIP clusters-based chain structures in the composite [35]. While the samples were cured, the sensors were divided into three different groups according to the direction of magnetic field, denoting 'random', 'horizontal', and 'vertical', respectively. For 'random' groups, the CNT@CIP clusters were randomly dispersed in the cementitious composites without applying magnetic field as shown in Fig. 1. The applied magnetic field at the side and center of the molds were about 200 and 100 mT, respectively. For 'horizontal' and 'vertical' groups, the direction of magnetic field and electrodes were horizontal and vertical, respectively as described in Fig. 1.

### 2.2. Experiment methods

To examine the formation of CNT@CIP-based nanohybrid clusters, various characterization methods were applied. A zeta potential analyzer (ELSZ-2000, Otsuka Electronics) was used to observe the relative surface charges of CNT and CIP, respectively. FT-IR and Raman spectra of the used fillers (e.g., CNT, CIP, and CNT@CIP clusters) were observed using a FTIR-7600 (Lambda scientific) and XperRam S (Nanobase Inc), respectively. In addition, microstructural images of each filler and CNT@CIP-based nanohybrid clusters were obtained using a field emission scanning electron microscope (FE-SEM, Hitachi S4800). Then, the DC and AC electrical characteristics of the samples were investigated using a portable multi-meter (U1281A, Keysightv.

Technologies) and LCR meter (IM3523, HIOKI), respectively, with a two-probe method. The piezoresistive sensing capabilities of the samples were investigated as the cyclic loadings were applied to the samples. The multipurpose servo-hydraulic universal testing machine (Walter Bai) was used to apply the sinusoidal loadings with 12.5 MPa and 0.25 Hz for 4 cycles in short-term loading test. In a long-term loading test, the loading with 10 MPa and 0.25 Hz was applied to the samples for 5000 cycles. During the cyclic loading tests, the electrical resistances of the samples were recorded using a digital multi-meter (Agilent Tech, 34410 A), and the measured electrical resistances were converted to the fractional change in electrical resistance (FCR) which expressed the sensitivity of the sensors.

## 3. Development of CNT@CIP-based nanohybrid clusters

In Table 1, the zeta potential values of CNT, CIP, and CNT@CIP in deionized water are summarized. The measured zeta potential values indicate the absolute values, and they were converted to the relative values as summarized in Table 1. The relative zeta potential values of CNT and CIP were 16.7 eV and − 13.0 eV, respectively, indicating that they were positively and negatively charged in the solution. The opposite charges indicated that the CIP can be wrapped with the CNT

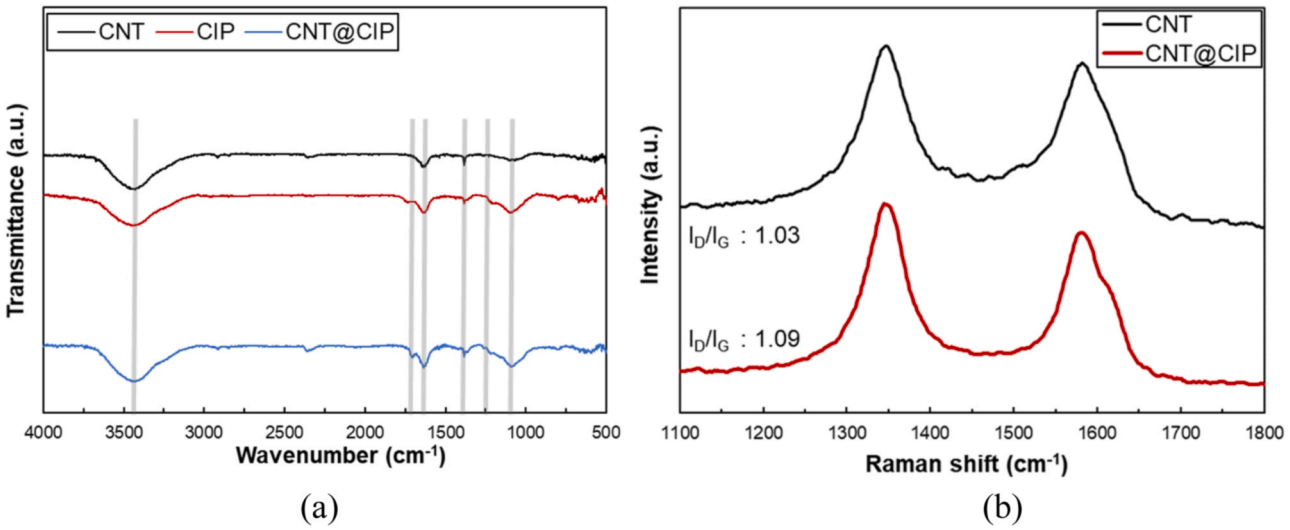


**Fig. 2.** (a) FT-IR spectra of CNT, CIP, and CNT@CIP-based nanohybrid clusters and (b) Raman spectra of CNT and CNT@CIP-based nanohybrid clusters.

particles, leading to the hybridization through the electrostatic interaction [36]. This hybridization of CNT and CIP was verified by the zeta potential values of CNT@CIP, showing intermediate surface charges (6.7 eV) of that observed in individual CNT and CIP. In addition, these zeta potential values can be used to quantify the stability of the colloidal dispersions of the materials. Here, the absolute zeta potential values of CNT, CIP, and CNT@CIP were − 17.3, − 47.0, and − 27.3 eV, respectively. It is generally accepted that the particles having zeta potential values greater than + 30 or less than − 30 mV can form stable colloidal dispersion. Therefore, the dispersion quality of CNT is relatively low, but that of CIP has a good dispersion property. In the case of CNT@CIP, the relatively low colloidal stability of CNT is compensated by hybridization with CIP, and thus CNT@CIP has an appropriate quality of colloidal dispersion.

The FT-IR spectra of CNT, CIP, and CNT@CIP are observed in Fig. 2a. For the CNT spectra, it showed notable peaks at 1089 $cm^{-1}$, 1255 $cm^{-1}$, 1382 $cm^{-1}$, 1635 $cm^{-1}$, 1706 $cm^{-1}$, and 3432 $cm^{-1}$. These peaks can be deduced from the C-O stretching, C-N stretching, O-H deformation, aromatic C═C stretching, C═O stretching, and O-H stretching, respectively [37,38]. For CIP spectra, the main peaks were observed at 1095 $cm^{-1}$, 1382 $cm^{-1}$, 1635 $cm^{-1}$, and 3438 $cm^{-1}$ from the C-O stretching, O-H deformation, C═O carbonyl stretching, and O-H stretching, respectively. As seen in Fig. 2a, a few oxygen-containing functional groups can be found in the FT-IR spectra of CNT and CIP. Hence, it can be asserted that they have a propensity to readily establish hydrogen bonds [31]. This expectation is verified by the FT-IR spectrum of CNT@CIP, showing a superposition of their individual features. The Raman spectra of CNT and CNT@CIP are exhibited in Fig. 2b. It indicates that CNT and CNT@CIP showed D peaks at 1348 and 1345 $cm^{-1}$, and G peak at 1583 and 1579 $cm^{-1}$, respectively. The relative intensity of D peak to G peak ($I_D/I_G$) was changed from 1.03 to 1.09 (Fig. 2b), indicating the crystallinity of graphitic carbon-based materials [38]. Therefore, based on the spectroscopic analyses, it can be said that the CNT particles are well hybridized with CIP, forming CNT@CIP-based nanohybrid clusters with strongly-interactive interfaces. In summary, the zeta potential analyzer was used to examine CNT and CIP nanohybridization based on the changes of their zeta potential values; since, if they form a hybrid structure, the zeta potential of the resulting hybrid can be the intermediate value between zeta potentials of CNT and CIP. FT-IR and Raman spectroscopies are representative vibration spectroscopies, and thus the peak shifts in FT-IR and Raman spectra can be directly related to the vibration transitions of chemical bonds through the chemical interactions [39]. If CNT and CIP can form a hybrid structure, the functional groups on their surface can interact multi-modally each other. The O-H stretching peaks of CNT and CIP were observed at 3453 and 3438 $cm^{-1}$, respectively. Interestingly, the O-H stretching peak of CNT@CIP was located at 3450 $cm^{-1}$, indicating there was hydrogen bonding between CNT and CIP to form strongly-interactive nanohybridized structures. The C═O stretching bond was not observed from CNT, but it was observed at 1731 $cm^{-1}$ from CIP which was shifted to 1708 $cm^{-1}$ from CNT@CIP. The shift of O-H and C═O stretching peaks implied those bonds were involved in formation of hydrogen bonding between CNT and CIP [40]. Likewise, Raman spectra of CNT, CIP, and CNT@CIP can also provide information about the interaction between CNT and CIP. The D and G peaks of CNT were observed at 1348 and 1583 $cm^{-1}$, and those peaks were shifted to

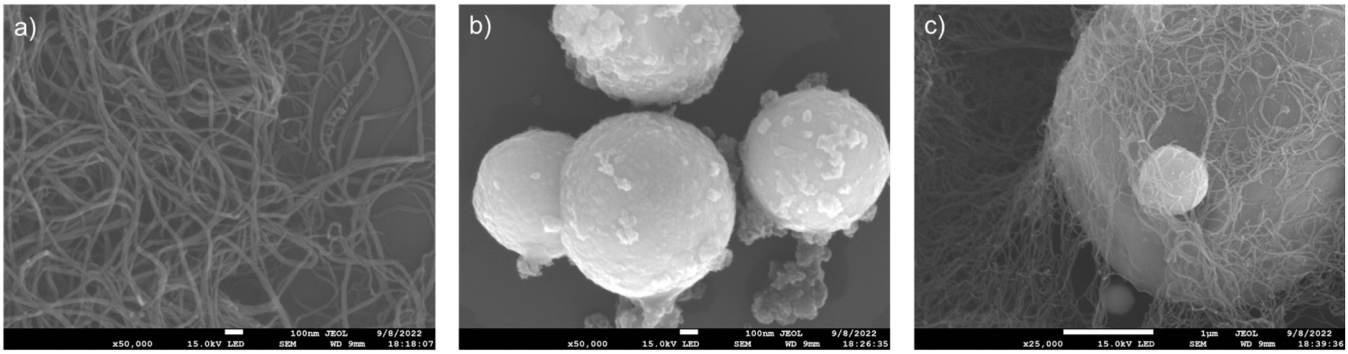


**Fig. 3.** SEM images of (a) CNT, (b) CIP, and (c) CNT@CIP-based nanohybrid clusters.

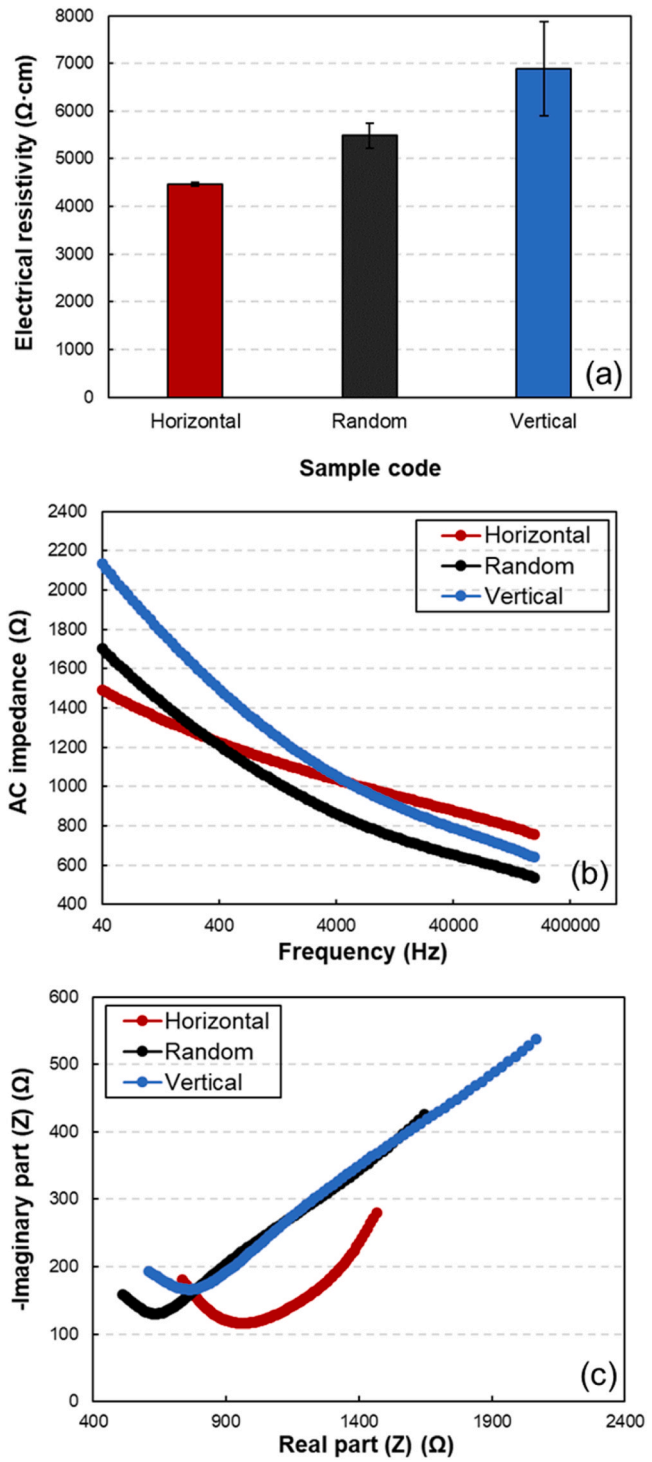


**Fig. 4.** (a) Electrical resistivities, (b) AC impedance, and (c) relationship between imaginary and real parts of the 'horizontal', 'random', and 'vertical' samples.

1345 and 1579 $cm^{-1}$ by nanohybridization with CIP. It is well known that Raman bands are affected by interfacial interaction, and thus the shift of D and G peaks of CNT indicated CNT were successfully nanohybridized with CIP [41]."

The SEM images of CNT, CIP, and CNT@CIP-based nanohybrid clusters are shown in Fig. 3. In Fig. 3a, it can be found that the diameter and length of CNT are approximately 15–40 nm and 100 μm, respectively. And, a broad size distribution from 500 nm to 5 μm can be seen in diameter of CIP. In addition, it can be confirmed that the CNT particles were attached to CIP, wrapping the CIP surfaces. The SEM images are in close agreement with the results of zeta potential analysis, confirming the formation of CNT@CIP-based nanohybrid clusters.

## 4. Electrical characteristics and piezoresistive sensing capability

The electrical resistances of the sensors were measured and the measured values were converted to electrical resistivity considering the size of the used electrodes as shown in Fig. 4. It can be observed that the magnetization curing affects the electrical characteristics of the sensors [42]. Specifically, the fact that the direction of magnetic field also affects the electrical characteristics of the sensors was found. 'Horizontal' sensors showed low electrical resistivity, while 'vertical' sensors showed high electrical resistivity compared to that of 'random' sensors (See Fig. 4a).

This phenomenon can be explained from the effects of CNT@CIP clusters-based conductive networks on the electrical conductivity of the samples. In the 'horizontal' sensors, the CNT@CIP clusters-based conductive networks formed well in the same direction of electrodes. This means that the electrons can easily move through the conductive networks when the electrical resistance of the sensors is measured, reducing the electrical resistivity [31]. However, in the 'vertical' sensors, the formed conductive networks are vertical to the direction of electron movements, hindering the movements of the electrons. For these reasons, the electrical resistivity of the 'vertical' sensors is higher than that of the 'random' sensors. Similar results can be found in the previous study by Park et al. [43]. They observed that the aligned chain structures of CIP can lead to the easy movement of the electrons; thus, it reduced the electrical resistance of the composites, which are in close agreement with the present test results [42,43]. In addition, this anisotropic electrical resistivity implied that the structure of CNT@CIP clusters were stably maintained during mixing with cementitious composites and magnetization curing because the anisotropic electrical resistivity originated from the alignment of CNT@CIP chains along with the magnetic field.

Meanwhile, the AC impedance of the samples and their Cole-Cole chart are exhibited in Figs. 4b and 4c, respectively. In these figures, the AC impedance of the sensors regardless of the direction of nanohybrid clusters-based chain structures decreased as the frequency increased, which are similar result to the previous study [43]. However, interestingly, the degree of decreasing AC impedance was different according to the direction of the formed chain structures. At the low frequency, the 'vertical' and 'horizontal' sensors showed high and low values of AC impedance compared to that of 'random' sensors, respectively. However, it changed as the frequency increased, indicating that the AC impedance of 'horizontal' sensor is higher than that of 'vertical' and 'random' sensors.

Fig. 5 shows an experimental setup for piezoresistive sensing test. The 'horizontal' and 'vertical' sensors were put on the plate, and the compressive loading applied to the samples, at the same time. From the multi-meter, the electrical resistance was measured, and the measured values were converted to the fractional change in electrical resistance. The piezoresistive sensing capabilities of the samples were shown in Fig. 6.

As seen in Fig. 6, it can be found that the degree of fractional change in electrical resistance was different according to the direction of CNT@CIP-based clusters. The 'horizontal' sensor showed higher electrical resistance change, while 'vertical' sensor showed lower electrical resistance change compared to the 'random' sensor. This result can be deduced from the direction of the formed CNT@CIP-based conductive networks in the sensor, which is explained in Fig. 4. The direction of the networks is same as the direction of the applied loading, leading to the continuous changes in electrical resistance when compressive loading is applied to the sensors. Whereas, the direction of network and applied loading is vertical in the 'vertical' sensor. Therefore, the changes of electrical resistance is much lower than 'random' and 'horizontal'

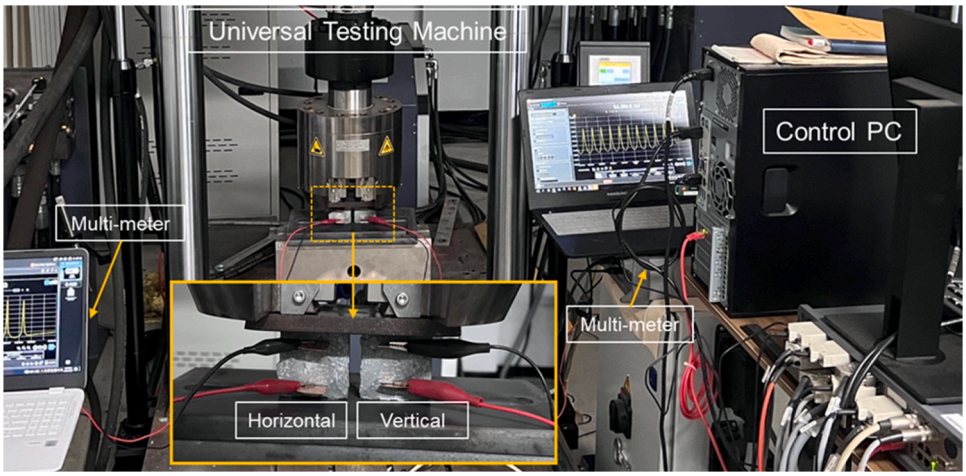


**Fig. 5. Experimental setup for multi-directional piezoresistive sensing test.**

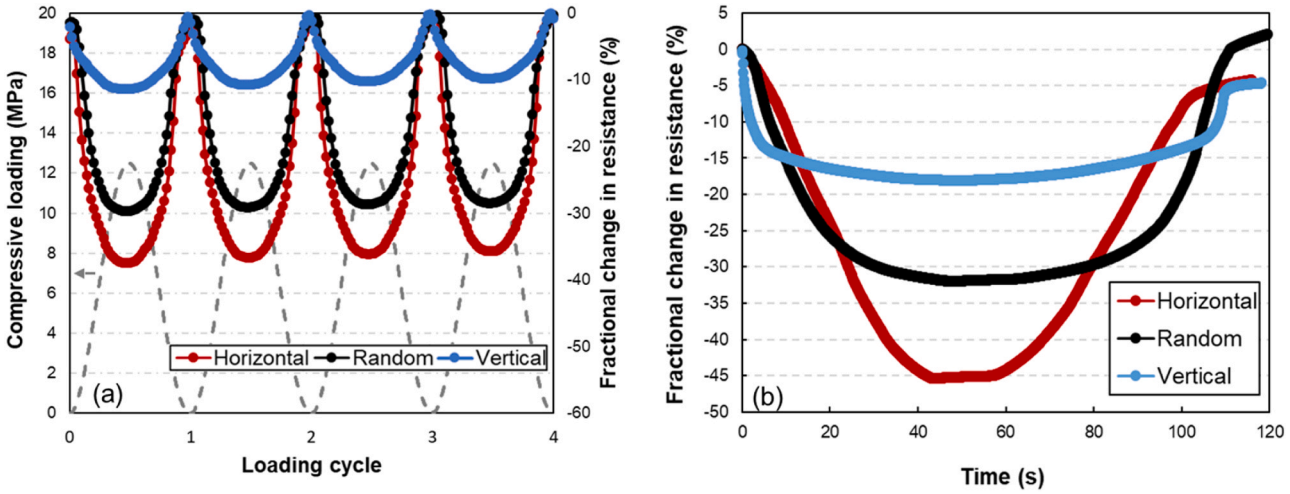


**Fig. 6.** Piezoresistive sensing test results under (a) cyclic and (b) monotonic loading conditions.

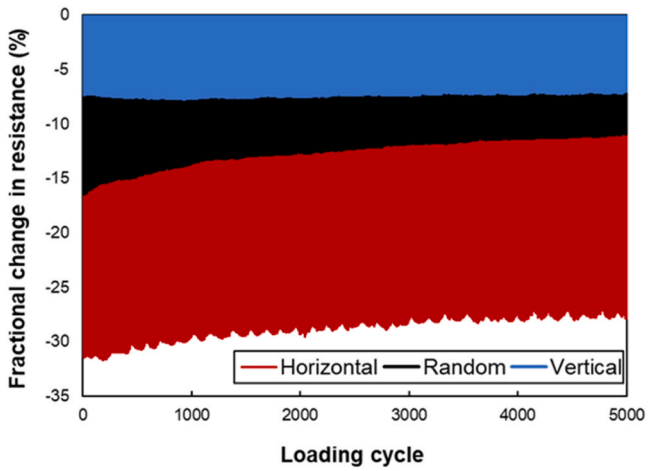


**Fig. 7.** Long-term piezoresistive sensing test results under 5000 cyclic loading condition.

sensors, leading to low sensitivity as seen in Fig. 6a. Meanwhile, the obtained fractional change in resistance values can be used to calculate the stress sensitivity (%/MPa). The horizontal, random, and vertical samples showed 3.12, 2.47, 0.98%/MPa of the stress sensitivity, respectively. As summarized in Seo et al., the stress sensitivity obtained in the previous studies are similar or lower than 1.5%/MPa [44]. Thus, it can be said that the fabricated sensor showed the outstanding stress sensitivity compared to those found in the previous studies.

Similar result can be seen in monotonic loading test as shown in Fig. 6b. In initial stage, the change of electrical resistance was much higher in 'vertical' sensor, leaching to the maximum value of electrical resistance change. However, the continuous changes of electrical resistance change was observed in the 'horizontal' sensor since the direction of applied loading is same as that of networks. Based on these piezoresistive sensors, the two different types of sensors showed different sensitivity compared to the sensor fabricated with normal curing method (i.e., 'random' sensor). Thus, the direction of applied loading can be predicted as same loading was applied to the 'horizontal', 'vertical', and 'random' sensors, respectively. In this regard, the authors can say that the sensors fabricated in the present study can be used in cement-based sensors with multi-directions, solving the problems of the conventional cement-based sensors for using in structural health monitoring sensors.

Meanwhile, the long-term piezoresistive sensing test results during 5000 cyclic loading condition are shown in Fig. 7. As depicted in Fig. 7, the 'horizontal' sample exhibited the highest FCR, followed by the 'random' and 'vertical' samples in order. The observed trends in FCR values with respect to the orientation of conductive networks are

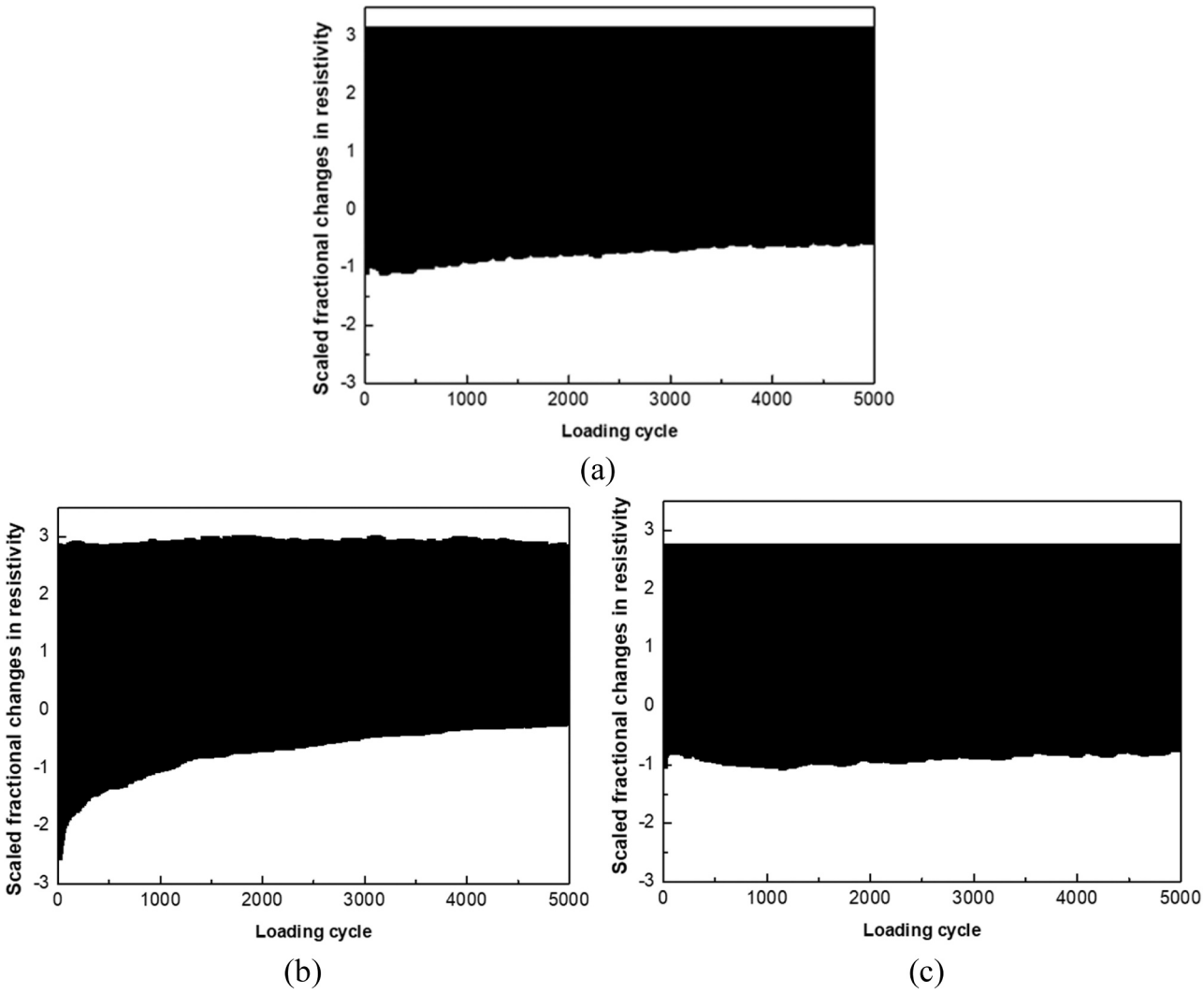


**Fig. 8.** Scaled piezoresistive sensing test results under cyclic loading condition: (a) Horizontal, (b) random, and (c) vertical samples.

consistent with the results presented in Figs. 4 and 5. Consequently, it is believed that the mechanism of FCR measured through repetitive cyclic loadings follows a similar context. However, as the number of loading cycles increases, the FCR magnitude of the 'random' and 'horizontal' samples slightly diminishes. This reduction is hypothesized to result from the accumulation of micro-damage due to repetitive loadings and the consequent changes in the internal structure of the samples.

## 5. Prediction of long-term sensing capability using LSTM model

A computational method for predicting the FCR in the composites using a deep learning based LSTM model is proposed. The LSTM model is a type of deep learning architecture specifically designed to handle sequential data by addressing the vanishing gradient problem [45,46]. Prior to implementing the LSTM deep learning model, the collected FCR data was preprocessed to facilitate efficient and stable model training. First, we converted the resistivity data into a suitable scale for LSTM analysis. Although data is typically scaled between − 1 and 1 for deep learning applications. However, in case of the data applied in this analysis were scaled within this range, the number of decimal places would increase, which would eventually lead to an increase in the amount of computation and a delay in the computation speed [47]. Hence, we opted for a range of − 3–3 for the present LSTM simulation as shown in Fig. 8.

Following data scaling, the experimental dataset was divided into two subsets: a training set comprising 3000 data points and a validation set consisting of the remaining 2000 data points. This partitioning allowed for the evaluation of the LSTM model's capability on previously unseen data. Then, a connected 128-single layer LSTM network was designed and implemented to predict the FCR in the samples under receptive compressive loads. The model's architecture and training parameters were optimized to enhance its prediction accuracy and generalization capability.

In the present of LSTM, two distinct prediction methods were considered: open loop and closed loop. In the open loop method, the LSTM model uses its own previous predictions as inputs for making future predictions. After training the LSTM model, an initial input sequence is fed into the model. It then generates a prediction for the next time step, which is subsequently used as input for predicting the following time step [48,49]. The closed loop prediction method, on the other hand, involves using the actual observed values from the ground truth as inputs for making predictions at each time step. In this method, the LSTM model generates a prediction for a specific time step based on the true value of the previous time step, rather than relying on its own previous predictions [48]. Herein, we compared the open loop and closed loop prediction methods in terms of their root mean square error (RMSE), which served as a measure of the model's capabilities. Fig. 9 shows the comparison of experimental measurements and LSTM analysis for each specimen, divided into open loop and closed loop.

The RMSE values predicted by the open loop LSTM for the

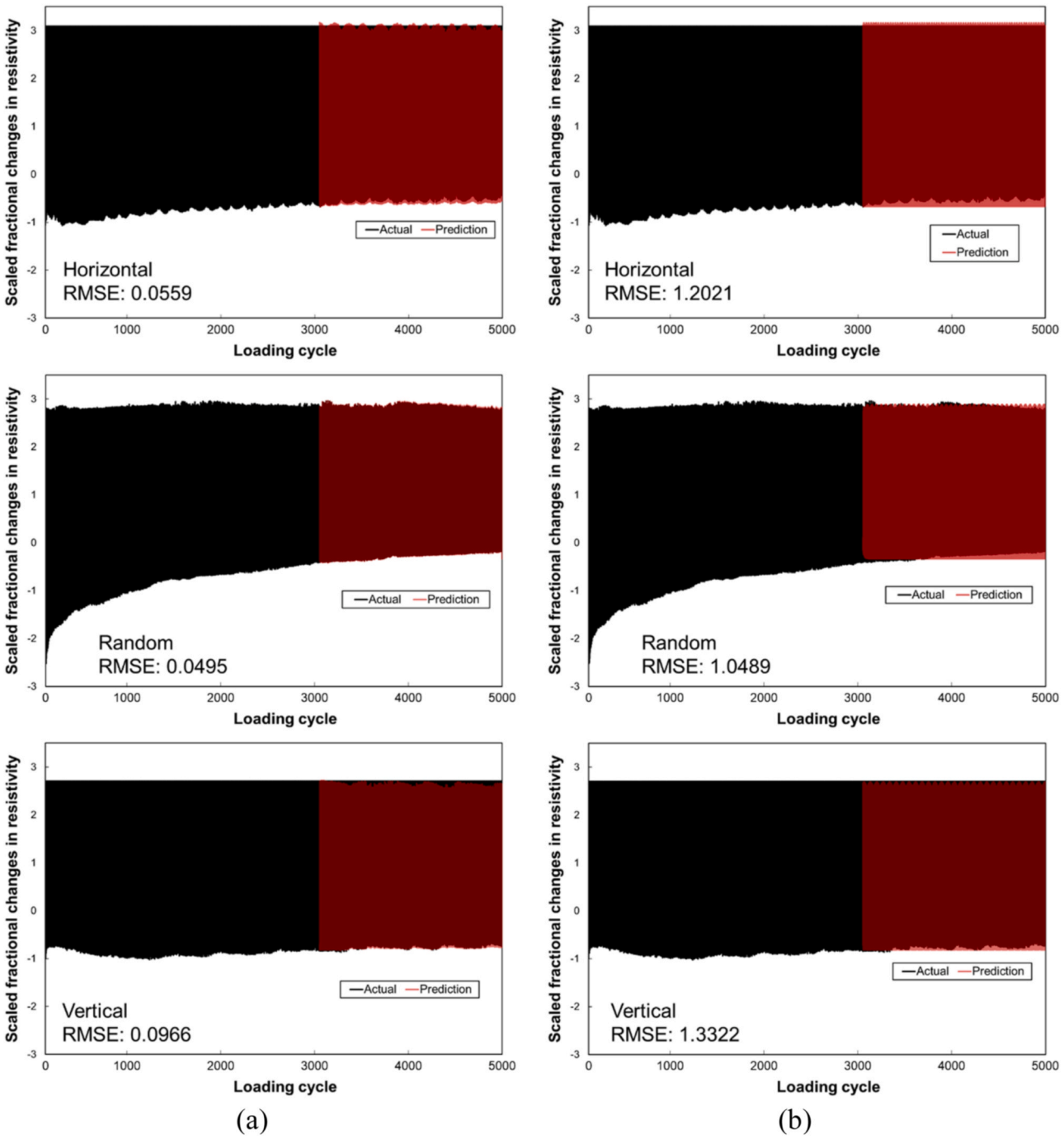


**Fig. 9.** The comparison of experimental measurements and LSTM analysis for each specimen (a) open loop and (b) closed loop.

horizontal, random, and vertical samples are 0.0797, 0.0495, and 0.0966, respectively; while the RMSE values predicted by the closed loop method for the same samples are 1.3932, 1.0489, and 1.4281, respectively. Therefore, for all samples, the open loop-based analysis produced more accurate predictions than the closed loop-based prediction. The difference in prediction accuracy between open loop and closed loop methods arises primarily due to the error accumulation. The closed loop methods exclusively rely on pre-trained data for forecasting subsequent sequences, thereby accruing errors over time and diminishing prediction accuracy. In contrast, the open loop methods continuously update the model with present observations to anticipate forthcoming sequences, thereby mitigating error accumulation. In overall, the results obtained from the LSTM deep learning model suggest

**Table 2**
Specifications and hyperparameter values applied to LSTM analysis.

| Index | Components |
|---|---|
| Epoch | 150 |
| Number of layer | 128 |
| Dropout ratio | 0.2 |
| Learning rate | 0.001 |
| Optimizer | Adam |
| Data scaling | -3–3 |
| Forecasting method | Open loop<br>Closed loop |

that it is capable of accurately predicting the piezoresistive capability of cement composites under cyclic compressive loads [50].

The prediction results presented above were obtained by applying optimized hyper-parameters derived through extensive numerical analysis. To provide a more comprehensive understanding of the applied parameters, we have summarized the detailed information regarding these hyper-parameters in Table 2. In an effort to promote further research in the field of using LSTM modeling for predicting long-term piezoresistive sensing capability of sensors, we have shared the MATLAB code and experimental measurement data used in this study. By providing these resources, we aim to facilitate the practical application of these composites, as well as the advancement of deep learning techniques for piezoresistive sensing prediction.

## 6. Conclusion

In this study, cement-based sensors which can detect both levels and direction of the applied loadings was developed. A new method for developing CNT@CIP-based nanohybrid clusters was introduced. The proposed clusters were added to the cement-based sensors and the orientation of conductive networks in the sensors was controlled by the magnetic field. Afterwards, the piezoresistive sensing capabilities of the sensors were investigated and their long-term sensing capabilities were predicted using the LSTM model. The main findings obtained in present study are summarized as follows.

1) The novel method for developing CNT@CIP-based nanohybrid clusters was proposed, and their formation was evaluated using various characterization methods.
2) The magnetization curing method was used to control the orientation of conductive networks in the cement-based sensors, and the different electrical conductivity of cement-based sensors according to differently aligned conductive networks was observed.
3) The possibility of developed cement-based sensors for using as multi-directional sensor was evaluated under the monotonic, cyclic, and long-term loading conditions.
4) LSTM model was used to predict the long-term sensing capabilities of the fabricated cement-based sensors using the experimental results, and their accuracy regarding their methods was compared.

The current experimental findings reveal that the sensors with differently aligned conductive networks exhibit different levels of sensing sensitivity when subjected to identical compressive loads. Consequently, it is anticipated that the applied load's direction can be discerned through a comparative analysis of the sensors' sensing sensitivity.

## CRediT authorship contribution statement

**Daeik Jang:** Conceptualization, Data curation, Formal analysis, Investigation, Methodology, Validation, Writing – original draft. **Jinho Bang:** Data curation, Investigation, Validation. **H.N. Yoon:** Conceptualization, Investigation, Methodology. **Young-Kwan Kim:** Data curation, Formal analysis, Investigation. **Jae Hyuk Lee:** Data curation, Formal analysis. **Hyungchul Yoon:** Data curation, Formal analysis, Validation. **Se-Hyun Cheon:** Data curation. **Beomjoo Yang:** Resources, Supervision, Writing – original draft, Writing – review & editing.

## Declaration of Competing Interest

The authors declare that they have no known competing financial interests or personal relationships that could have appeared to influence the work reported in this paper.

## Data availability

Data will be made available on request.

## Acknowledgment

This study was supported by the National Research Foundation of Korea (NRF) grant funded by the Korea government (MSIT) (2020R1C1C1005063).

## Appendix A. Supporting information

Supplementary data associated with this article can be found in the online version at doi:10.1016/j.conbuildmat.2023.134116.

## References

[1] D. Jang, H.N. Yoon, B. Yang, J. Seo, S.Z. Farooq, H.K. Lee, Synergistic effects of CNT and CB inclusion on the piezoresistive sensing behaviors of cementitious composites blended with fly ash, Smart Struct. Syst. 2 (2022) 351–359.
[2] Y. Guo, W. Li, W. Dong, K. Wang, X. He, K. Vessalas, D. Sheng, Self-sensing cement-based sensors with superhydrophobic and self-cleaning capacities after silane-based surficial treatments, Case Stud. Constr. Mater. 17 (2022), e01311, https://doi.org/10.1016/j.cscm.2022.e01311.
[3] W. Li, W. Dong, Y. Guo, K. Wang, S.P. Shah, Advances in multifunctional cementitious composites with conductive carbon nanomaterials for smart infrastructure, Cem. Concr. Compos 128 (2022), 104454, https://doi.org/10.1016/j.cemconcomp.2022.104454.
[4] Z. Tian, Y. Li, J. Zheng, S. Wang, A state-of-the-art on self-sensing concrete: materials, fabrication and properties, Compos B Eng. 177 (2019), 107437, https://doi.org/10.1016/j.compositesb.2019.107437.
[5] S. Ding, X. Wang, L. Qiu, Y.Q. Ni, X. Dong, Y. Cui, A. Ashour, B. Han, J. Ou, Self-sensing cementitious composites with hierarchical carbon fiber-carbon nanotube composite fillers for crack development monitoring of a maglev girder, Small 19 (2023), https://doi.org/10.1002/smll.202206258.
[6] S. Ding, Y. Xiang, Y.Q. Ni, V.K. Thakur, X. Wang, B. Han, J. Ou, In-situ synthesizing carbon nanotubes on cement to develop self-sensing cementitious composites for smart high-speed rail infrastructures, Nano Today 43 (2022), 101438, https://doi.org/10.1016/j.nantod.2022.101438.
[7] D. Jang, H.N. Yoon, S. Park, S. Kim, J.H. Bae, N. Kim, G.M. Kim, J. Seo, Pressure-aided fabrication of CNT-incorporated composites made with fly ash or slag-blended Portland cement, Compos Struct. 313 (2023), 116926, https://doi.org/10.1016/j.compstruct.2023.116926.
[8] A. Abolhasani, A. Pachenari, S. Mohammad Razavian, M. Mahdi Abolhasani, Towards new generation of electrode-free conductive cement composites utilizing nano carbon black, Constr. Build. Mater. 323 (2022), 126576, https://doi.org/10.1016/j.conbuildmat.2022.126576.
[9] W. Dong, W. Li, Y. Guo, F. Qu, K. Wang, D. Sheng, Piezoresistive performance of hydrophobic cement-based sensors under moisture and chloride-rich environments, Cem. Concr. Compos 126 (2022), 104379, https://doi.org/10.1016/j.cemconcomp.2021.104379.
[10] W. Li, F. Qu, W. Dong, G. Mishra, S.P. Shah, A comprehensive review on self-sensing graphene/cementitious composites: A pathway toward next-generation smart concrete, Constr. Build. Mater. 331 (2022), 127284, https://doi.org/10.1016/j.conbuildmat.2022.127284.
[11] H.N. Yoon, D. Jang, T. Kil, H.K. Lee, Influence of various deterioration factors on the electrical properties of conductive cement paste, Constr. Build. Mater. 367 (2023), 130289, https://doi.org/10.1016/j.conbuildmat.2022.130289.
[12] D. Jang, H.N. Yoon, B. Yang, H.R. Khalid, Cyclic heat-generation and storage capabilities of self-heating cementitious composite with an addition of phase change material, Constr. Build. Mater. 369 (2023), 130512, https://doi.org/10.1016/j.conbuildmat.2023.130512.
[13] A.R.Mahtab Mardani, Seyed Hossein Hosseini Lavassani, Mostafa Adresi, Piezoresistivity and mechanical properties of self- sensing CNT cementitious nanocomposite: optimizing the effects of cnt dispersion and surfactants, Constr. Build. Mater. 349 (2022), 128127, https://doi.org/10.2139/ssrn.4078405.
[14] W. Dong, W. Li, K. Wang, B. Han, D. Sheng, S.P. Shah, Investigation on physicochemical and piezoresistive properties of smart MWCNT/cementitious composite exposed to elevated temperatures, Cem. Concr. Compos 112 (2020), 103675, https://doi.org/10.1016/j.cemconcomp.2020.103675.
[15] M. Tafesse, A. Shiferaw, H. Kyoung, C. Cho, H. Kim, Effect of chloride penetration on electrical resistivity of CNT – CF / cement composites and its application as chloride sensor for reinforced mortar, Cem. Concr. Compos 133 (2022), 104662, https://doi.org/10.1016/j.cemconcomp.2022.104662.
[16] O. Öztürk, G. Yıldırım, Ü.S. Keskin, H. Siad, M. Şahmaran, Nano-tailored multi-functional cementitious composites, Compos B Eng. 182 (2020), https://doi.org/10.1016/j.compositesb.2019.107670.
[17] M. Tafesse, N. Kon, A. Shiferaw, H. Kyoung, S. Wook, H. Kim, Flowability and electrical properties of cement composites with mechanical dispersion of carbon nanotube, Constr. Build. Mater. 293 (2021), 123436, https://doi.org/10.1016/j.conbuildmat.2021.123436.

[18] M.S. Konsta-Gdoutos, Z.S. Metaxa, S.P. Shah, Highly dispersed carbon nanotube reinforced cement based materials, Cem. Concr. Res 40 (2010) 1052–1059, https://doi.org/10.1016/j.cemconres.2010.02.015.
[19] A. Sobolkina, V. Mechtcherine, V. Khavrus, D. Maier, M. Mende, M. Ritschel, A. Leonhardt, Dispersion of carbon nanotubes and its influence on the mechanical properties of the cement matrix, Cem. Concr. Compos 34 (2012) 1104–1113, https://doi.org/10.1016/j.cemconcomp.2012.07.008.
[20] L.I. Nasibulina, I.V. Anoshkin, A.G. Nasibulin, A. Cwirzen, V. Penttala, E. I. Kauppinen, Effect of carbon nanotube aqueous dispersion quality on mechanical properties of cement composite, J. Nanomater 2012 (2012), https://doi.org/10.1155/2012/169262.
[21] D. Jang, H.N. Yoon, J. Seo, H.K. Lee, G.M. Kim, Effects of silica aerogel inclusion on the stability of heat generation and heat-dependent electrical characteristics of cementitious composites with CNT, Cem. Concr. Compos 115 (2021), 103861, https://doi.org/10.1016/j.cemconcomp.2020.103861.
[22] Y. Gao, H.W. Jing, S.J. Chen, M.R. Du, W.Q. Chen, W.H. Duan, Influence of ultrasonication on the dispersion and enhancing effect of graphene oxide–carbon nanotube hybrid nanoreinforcement in cementitious composite, Compos B Eng. 164 (2019) 45–53, https://doi.org/10.1016/j.compositesb.2018.11.066.
[23] D. Jang, H.N. Yoon, J. Seo, B. Yang, Effects of exposure temperature on the piezoresistive sensing performances of MWCNT-embedded cementitious sensor, J. Build. Eng. 47 (2022), 103816, https://doi.org/10.1016/j.jobe.2021.103816.
[24] Y. Wang, X. Zhao, Y. Zhao, Piezoresistivity of cement matrix composites incorporating multiwalled carbon nanotubes due to moisture variation, Adv. Civ. Eng. 2020 (2020), https://doi.org/10.1155/2020/5476092.
[25] D. Jang, H.N. Yoon, S.Z. Farooq, H.K. Lee, I.W. Nam, Influence of water ingress on the electrical properties and electromechanical sensing capabilities of CNT / cement composites, J. Build. Eng. 42 (2021), 103065, https://doi.org/10.1016/j.jobe.2021.103065.
[26] M.K. Hassanzadeh-Aghdam, M.J. Mahmoodi, M. Safi, Effect of adding carbon nanotubes on the thermal conductivity of steel fiber-reinforced concrete, Compos B Eng. 174 (2019), 106972, https://doi.org/10.1016/j.compositesb.2019.106972.
[27] J. Donnini, T. Bellezze, V. Corinaldesi, Mechanical, electrical and self-sensing properties of cementitious mortars containing short carbon fibers, J. Build. Eng. 20 (2018) 8–14, https://doi.org/10.1016/j.jobe.2018.06.011.
[28] Z. Tian, S. Li, Y. Li, Aligning conductive particles using magnetic field for enhanced piezoresistivity of cementitious composites, Constr. Build. Mater. 313 (2021), 125582, https://doi.org/10.1016/j.conbuildmat.2021.125582.
[29] Z. Tian, S. Li, Y. Li, Enhanced sensing performance of cement-based composites achieved via magnetically aligned nickel particle network, Compos. Commun. 29 (2022), 101006, https://doi.org/10.1016/j.coco.2021.101006.
[30] Z. Tian, Y. Li, S. Li, S. Vute, J. Ji, Influence of particle morphology and concentration on the piezoresistivity of cement-based sensors with magneto-aligned nickel fillers, Meas. (Lond. ) 187 (2022), 110194, https://doi.org/10.1016/j.measurement.2021.110194.
[31] D. Jang, H.N. Yoon, J. Seo, H.J. Cho, G.M. Kim, Y.-K. Kim, B. Yang, Improved electromagnetic interference shielding performances of carbon nanotube and carbonyl iron powder (CNT@CIP)-embedded polymeric composites, J. Mater. Res. Technol. 18 (2022) 1256–1266, https://doi.org/10.1016/j.jmrt.2022.02.134.
[32] M. Tomás, S. Jalali, K. Tabatha, A deep neural network for electrical resistance calibration of self-sensing carbon fiber polymer composites compatible with edge computing structural monitoring hardware electronics, Struct. Health Monit. (2023), https://doi.org/10.1177/14759217231170001.
[33] L. Chen, H. Hassan, T.N. Tallman, S.S. Huang, D. Smyl, Predicting strain and stress fields in self-sensing nanocomposites using deep learned electrical tomography, Smart Mater. Struct. 31 (2022), https://doi.org/10.1088/1361-665X/ac585f.
[34] D. Jang, H.N. Yoon, J. Seo, B. Yang, J.G. Jang, S. Park, Effect of carbonation curing regime on electric heating performance of CNT/cement composites, J. Build. Eng. 73 (2023), 106815, https://doi.org/10.1016/j.jobe.2023.106815.
[35] D.I. Jang, G.E. Yun, J.E. Park, Y.K. Kim, Designing an attachable and power-efficient all-in-one module of a tunable vibration absorber based on magnetorheological elastomer, Smart Mater. Struct. 27 (2018), https://doi.org/10.1088/1361-665X/aacdbd.
[36] G.M. Kim, T. Kil, H.K. Lee, A novel physicomechanical approach to dispersion of carbon nanotubes in polypropylene composites, Compos Struct. 258 (2021), 113377, https://doi.org/10.1016/j.compstruct.2020.113377.
[37] J. Jeon, M. Choi, S.B. Kim, T.H. Seo, B.C. Ku, S. Ryu, J.H. Park, Y.K. Kim, Eggshell membrane hydrolysate as a multi-functional agent for synthesis of functionalized graphene analogue and its catalytic nanocomposites, J. Ind. Eng. Chem. 102 (2021) 233–240, https://doi.org/10.1016/j.jiec.2021.07.010.
[38] C.J. Yoon, S.H. Lee, Y. Bin Kwon, K. Kim, K.H. Lee, S.M. Kim, Y.K. Kim, Fabrication of sustainable and multifunctional TiO2@carbon nanotube nanocomposite fibers, Appl. Surf. Sci. 541 (2021), 148332, https://doi.org/10.1016/j.apsusc.2020.148332.
[39] J. Chen, L. Yan, W. Song, D. Xu, Interfacial characteristics of carbon nanotube-polymer composites: a review, Compos Part A Appl. Sci. Manuf. 114 (2018) 149–169, https://doi.org/10.1016/j.compositesa.2018.08.021.
[40] A. Rasheed, H.G. Chae, S. Kumar, M.D. Dadmun, Polymer nanotube nanocomposites: correlating intermolecular interaction to ultimate properties, Polym. (Guildf. ) 47 (2006) 4734–4741, https://doi.org/10.1016/j.polymer.2006.04.016.
[41] X. Yan, T. Suzuki, Y. Kitahama, H. Sato, T. Itoh, Y. Ozaki, A study on the interaction of single-walled carbon nanotubes (SWCNTs) and polystyrene (PS) at the interface in SWCNT-PS nanocomposites using tip-enhanced Raman spectroscopy, Phys. Chem. Chem. Phys. 15 (2013) 20618–20624, https://doi.org/10.1039/c3cp53859a.
[42] D. Jang, Y. Kim, T. Lim, H. Cheng, J. Wonsuk, Effects of carbon nanotube and graphene oxide incorporation on the improvements of magneto-induced electrical sensitivity of magneto-rheological gel, Polym. (Basel) 14 (2022) 5286.
[43] J.E. Park, G.E. Yun, D.I. Jang, Y.K. Kim, Analysis of electrical resistance and impedance change of magnetorheological gels with DC and AC voltage for magnetometer application, Sens. (Switz. ) 19 (2019), https://doi.org/10.3390/s19112510.
[44] J. Seo, D. Jang, B. Yang, H.N. Yoon, J.G. Jang, S. Park, H.K. Lee, Material characterization and piezoresistive sensing capability assessment of thin-walled CNT-embedded ultra-high performance concrete, Cem. Concr. Compos 134 (2022), 104808, https://doi.org/10.1016/j.cemconcomp.2022.104808.
[45] H. Abbasimehr, R. Paki, Improving time series forecasting using LSTM and attention models, J. Ambient Intell. Humaniz Comput. 13 (2022) 673–691, https://doi.org/10.1007/s12652-020-02761-x.
[46] Y. Liu, D. Hou, J. Bao, Y. Qi, Multi-step ahead time series forecasting for different data patterns based on LSTM recurrent neural network, Proceedings - 2017 14th Web Information Systems and Applications Conference, WISA 2017. 2018-Janua (2018) 305–310, https://doi.org/10.1109/WISA.2017.25.
[47] Y. Ensafi, S.H. Amin, G. Zhang, B. Shah, Time-series forecasting of seasonal items sales using machine learning – a comparative analysis, Int. J. Inf. Manag. Data Insights 2 (2022), 100058, https://doi.org/10.1016/j.jjimei.2022.100058.
[48] F. Elmaz, R. Eyckerman, W. Casteels, S. Latré, P. Hellinckx, CNN-LSTM architecture for predictive indoor temperature modeling, Build. Environ. 206 (2021), 108327, https://doi.org/10.1016/j.buildenv.2021.108327.
[49] Y. Chen, Voltages prediction algorithm based on LSTM recurrent neural network, Opt. (Stuttg. ) 220 (2020), 164869, https://doi.org/10.1016/j.ijleo.2020.164869.
[50] B.J. Yang, J.U. Jang, S.H. Eem, S.Y. Kim, A probabilistic micromechanical modeling for electrical properties of nanocomposites with multi-walled carbon nanotube morphology, Compos Part A Appl. Sci. Manuf. 92 (2017) 108–117, https://doi.org/10.1016/j.compositesa.2016.11.009.